

Cite this: *CrystEngComm*, 2012, 14, 7780–7786

www.rsc.org/crystengcomm

PAPER

5,10,15,20-tetra(4-pyridyl)porphyrinato zinc coordination polymeric particles with different shapes and luminescent properties†

Wei Sun,^a Hailong Wang,^a Dongdong Qi,^a Liang Wang,^a Kang Wang,^a Jinglan Kan,^a Wenjun Li,^{*a} Yanli Chen^{*b} and Jianzhuang Jiang^a

Received 10th February 2012, Accepted 26th April 2012

DOI: 10.1039/c2ce25187f

Micro-scale three-dimensional coordination polymer particles (CPPs) have been synthesized from the surfactant-assisted reaction of $\text{Zn}(\text{OAc})_2 \cdot 2\text{H}_2\text{O}$ and 5,10,15,20-tetra(4-pyridyl)porphyrin (H_2TPyP) in DMF. The three-dimensional (3D) micro-prisms and micro-octahedra of the CPPs were obtained at different temperatures as found by scanning electron microscopy (SEM), high-resolution transmission electron microscopy (HRTEM) and a statistical analysis of the size distribution results. X-Ray diffraction (XRD) analysis revealed a circular hexametric cage structure cross-linked by a Zn–N axial coordination of the pyridyl ligands inside the micro-scale CPPs. Further support for this coordination polymerization mode of the micro-CPPs came from IR spectroscopy. The UV–vis spectra clearly show the formation of J-type aggregates in both the microstructures. The micro-CPPs show a stronger luminescence intensity over the individual porphyrin molecules, which is presumably due to the high surface area of the ZnTPyP-CPPs. Nevertheless, nitrogen adsorption/desorption isotherm measurements were performed to confirm the larger surface area and increased porosity of the micro-prisms and micro-octahedra relative to the self-assembled micro-rods of ZnTPyP, indicating the potential application of the two CPPs microstructures in the field of gas adsorption. The surfactant-assisted synthetic route appears to provide a promising method for the construction of highly organized three-dimensional organic micro-structures of 5,10,15,20-tetra(4-pyridyl)porphyrin derivatives.

Introduction

Nano-scale coordination polymer particles (CPPs) have received a great deal of attention due to their characteristic properties and useful applications in gas storage, optics, catalysis and as sensors.^{1–5} In comparison with metal–organic frameworks (MOFs), classic metal oxides and carbon-based materials, CPPs in the micro/nano-meter range usually exhibit specific advantageous properties.^{6–9} Different pathways have been developed for the generation of micro/nano-scaled CPPs, including precipitation, solvothermal and reverse microemulsion methods.^{10–12} In particular, a variety of CPPs based on In(III) and O,N-donor ligands with controlled morphologies and functionalities have been prepared by Oh and co-workers.¹³ By means of bis-metallo-tridentate Schiff base ligands and metal acetates of Zn(II), Cu(II) and Ni(II), nano-scale infinite coordination polymers (ICPs) have

been prepared by the group of Mirkin.⁴ However, the nano-scale CPPs of transition metals appear to still be limited to small molecular ligands, such as 1,4-benzenedicarboxylate (BDC) and 2,6-bis[(4-carboxyanilino)carbonyl]pyridine. The fabrication of CPPs using macrocyclic molecular ligands, like porphyrins, seems, to the best of our knowledge, to still be scarce.

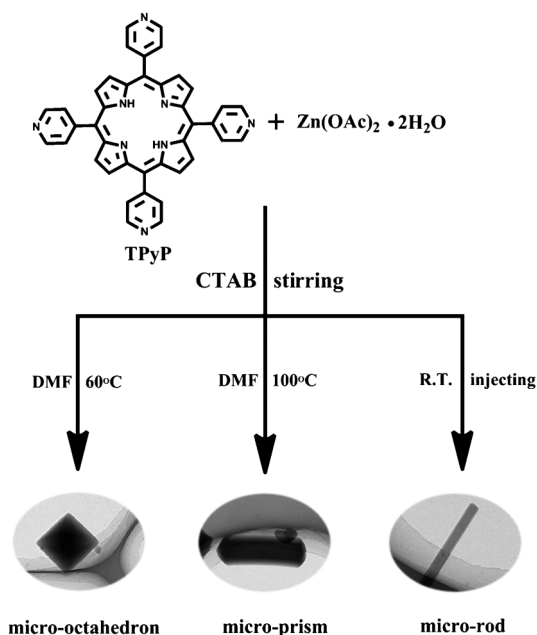
Meso-pyridyl attached porphyrins, such as the 5,10,15,20-tetra(4-pyridyl)porphyrin derivatives, have been widely utilized in the construction of metal organic frameworks¹⁴ and multi-porphyrin arrays,¹⁵ depending on the central metal–N axial coordination bonding interaction. In particular, both nano-plates and nano-prisms with a uniform size have been fabricated recently from CuTPyP, dependent mainly on the π – π interaction.¹⁶ As a result, the fabrication of CPPs of 5,10,15,20-tetra(4-pyridyl)porphyrinato metal complexes, in particular those with a tunable morphology and well-defined size, seems interesting considering the size/shape-dependent properties of micro-structures. In the present paper, we describe the preparation, luminescent properties and absorption of micro-sized CPPs of ZnTPyP with well-controlled shapes and a uniform size.

As can be seen in Scheme 1, the reaction between $\text{Zn}(\text{OAc})_2 \cdot 2\text{H}_2\text{O}$ and 5,10,15,20-tetra(4-pyridyl)porphyrin (H_2TPyP) in DMF with the help of a surfactant, cetyltrimethylammonium bromide (CTAB), results in the isolation of three-dimensional

^aDepartment of Chemistry, University of Science and Technology Beijing, Beijing, 100083, P. R. China. E-mail: wjli@sas.ustb.edu.cn; Fax: +86 (0) 010 6233 2462; Tel: +86 (0) 010 6233 2592

^bShandong Provincial Key Laboratory of Fluorine Chemistry and Chemical Materials, School of Chemistry and Chemical Engineering, University of Jinan, Jinan, 250022, P. R. China. E-mail: chm_chenyl@ujn.edu.cn; Fax: +86 (0) 0531 8973 6150; Tel: +86 (0) 0531 8973 6150

† Electronic Supplementary Information (ESI) available: characterization of the material. See DOI: 10.1039/c2ce25187f



Scheme 1 A reaction scheme for the preparation of micro-prism and micro-octahedron coordination polymer particles and self-assembled micro-rods.

(3D) micro-prisms and micro-octahedra of the CPPs at 60 and 100 °C, respectively, indicating the effect of the temperature and CTAB on the morphology of the micro-scaled CPPs. For comparison purposes, 1D self-assembled micro-rods were used as a reference material.

Experimental

Chemicals and measurements

DMF was freshly distilled just before use. Column chromatography was carried out on silica gel (Merck, Kieselgel 60, 200–300 mesh) with the indicated eluents. 5,10,15,20-Tetra(4-pyridyl) porphyrin (H_2TPyP , >99.9% ee) was purchased from Aldrich. All the other chemicals were of reagent grade and used as received without further purification.

Powder X-ray diffraction (PXRD) data were collected on a Shimadzu XRD-6000 diffractometer using $Cu-K\alpha$ radiation ($\lambda = 1.54056 \text{ \AA}$) at room temperature. Fourier-transform infrared (FT-IR) spectra were obtained on a Bruker Vector 22 FT-IR spectro-photometer using KBr pellets. UV–vis absorption spectra were measured on a UV-3600 spectrometer. The morphology of the as-prepared samples and the corresponding energy dispersive X-ray (EDX) spectroscopy were obtained with a JEOL JEM-6510A scanning electron microscope (SEM). High resolution transmission electron microscopy (HR-TEM) images were captured on a TECNAI F-20 microscope at an acceleration voltage of 200 kV. N_2 adsorption/desorption isotherms of the samples were obtained on a Micromeritics ASAP 2020 sorptometer at 77 K. All samples were outgassed prior to analysis at 343 K for 48 h under 10^{-4} Pa vacuum. Steady-state fluorescence spectroscopic studies were performed on a Hitachi F 4500. The slit width was 5 nm for the emission. The photon multiplier voltage was 700 V.

Preparation of the coordination polymer particles

Synthesis of ZnTPyP. A mixture of $Zn(OAc)_2 \cdot 2H_2O$ (100 mg, 0.46 mmol) and H_2TPyP (70 mg, 0.11 mmol) in $CHCl_3$ (0.5 mL) was heated at reflux for 1 h under nitrogen. After being cooled to room temperature, the mixture was chromatographed on a silica gel column. Following the recovery of the first violet band containing unreacted H_2TPyP with $CHCl_3$ as the eluent, the second red band containing the target ZnTPyP developed and was collected using $CHCl_3/CH_3OH$ (3 : 1) as an eluent. Repeated chromatography followed by recrystallization from $CHCl_3$ and MeOH gave a bright violet powder (67.25 mg, 96.1% yield).

Preparation of micro-prisms. A mixture of H_2TPyP (6.19 mg, 1 mmol), $Zn(OAc)_2 \cdot 2H_2O$ (10.98 mg, 5 mmol), and CTAB (36.45 mg, 0.01 mmol) in DMF (10 mL) was heated at 100 °C under vigorous stirring for 6 h. The purple solid was collected by centrifugation and washed with DMF and ethanol for three times.

Preparation of micro-octahedra. A mixture of H_2TPyP (6.19 mg, 1 mmol), $Zn(OAc)_2 \cdot 2H_2O$ (10.98 mg, 5 mmol) and CTAB (36.45 mg, 0.01 mmol) in DMF (10 mL) was heated at 60 °C under vigorous stirring for 6 h. The purple solid was collected by centrifugation and washed with DMF and ethanol three times.

Preparation of self-assembled ZnTPyP micro-rods. ZnTPyP in DMF (0.5 mL, 0.01 M) was quickly injected into 10 mL of an aqueous solution containing CTAB (36.45 mg, 0.01 mmol) under vigorous stirring at room temperature. The purple solid was collected by centrifugation and washed with water and ethanol three times.

Results and discussion

UV–vis spectra

Fig. 1 compares the electronic absorption spectra of ZnTPyP in DMF, its micro-prisms, micro-octahedra and self-assembled micro-rods dispersed in water. The absorption around 423 nm for ZnTPyP can be attributed to the porphyrin Soret band, while the two weak absorptions at 557 and 597 nm can be assigned to the Q bands. As can be seen from this figure, the single Soret band for ZnTPyP in DMF splits into two bands with the peak with a relatively weaker intensity appearing at 421 nm and the one with a stronger intensity appearing at 456 nm for the micro-prisms of ZnTPyP. Nevertheless, the two Q bands for ZnTPyP in DMF shift to a lower energy (571 and 610 nm) for the ZnTPyP micro-prisms in solution. These results suggest the formation of J-type aggregates with an edge-to-edge molecular arrangement in the micro-prism CPPs of ZnTPyP.^{17,18} This is also true for the self-assembled ZnTPyP micro-rods according to the observation of a relatively weaker Soret band at 416 nm and a stronger Soret band at 454 nm as well as the red-shifted Q bands at 570 and 610 nm.

Similar to the micro-prisms and self-assembled micro-rods, the two parts of the Soret band, with a shoulder at 407 nm and a main peak at 447 nm, were also observed in the electronic

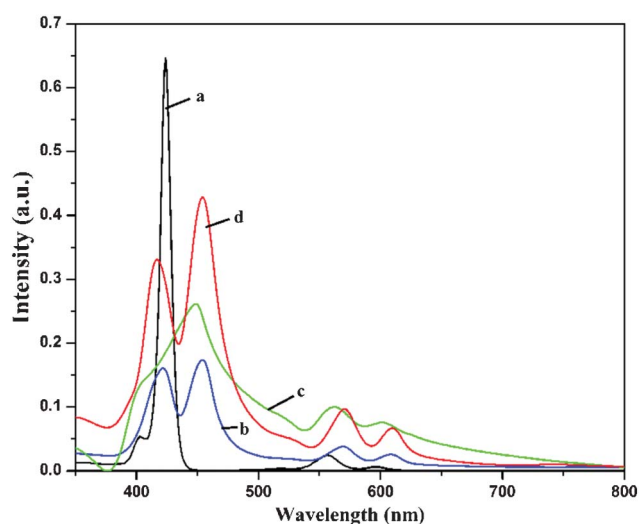


Fig. 1 The electronic absorption spectra of ZnTPyP (a) in DMF, ZnTPyP micro-prisms (b), ZnTPyP micro-octahedra (c) and self-assembled ZnTPyP micro-rods (d) dispersed in water.

absorption spectrum of the micro-octahedra (Fig. 1), which indicates that J-type aggregates exist in the micro-octahedra. Furthermore, the slightly red-shifted Q bands observed at 561 and 603 nm, in comparison to those of ZnTPyP in DMF, also provide evidence for the formation of J-aggregates in the micro-octahedra. The electronic absorption data of the different ZnTPyP microstructures is shown in Table 1. These results seem to indicate the similar aggregation properties of the ZnTPyP molecules when they appear in micro-octahedra, micro-prisms and self-assembled ZnTPyP micro-rods.

However, the degrees to which the absorption spectra shift for both the Soret and Q bands of the micro-prisms, micro-octahedra and self-assembled micro-rods from the spectra of ZnTPyP in solution are different, indicating the effect of the various molecular interactions on the molecular packing conformation in the aggregates due to the introduction of the surfactant, CTAB. Further evidence for this point comes from the FT-IR, XRD and photoluminescence (PL) emission spectra as detailed below.

Morphology

The external morphology and size of the ZnTPyP coordination polymer particles (CPPs) were characterized by scanning electron microscopy (SEM) and transmission electron microscopy (TEM). As shown in Fig. 2A, 2B and 2C, large scale and uniformly sized three-dimensional CPP structures were obtained

Table 1 The electronic absorption data for ZnTPyP in DMF, together with those of the ZnTPyP micro-prisms, micro-octahedra and self-assembled micro-rods dispersed in water

Compound	λ max/nm	
	Soret bands	Q bands
ZnTPyP in DMF	423	557, 597
micro-prisms	421, 456	571, 610
micro-octahedra	407, 447	561, 603
micro-rods	416, 454	570, 610

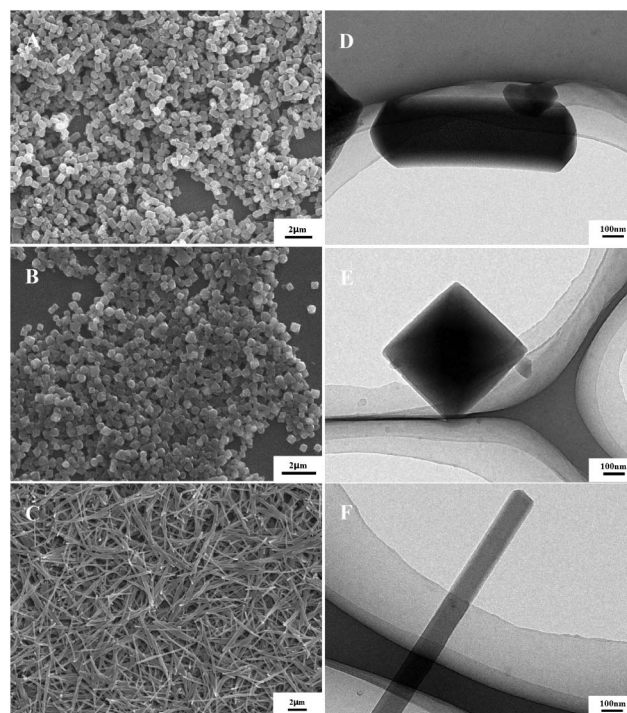


Fig. 2 SEM images of the micro-prisms (A) and micro-octahedra (B) formed with CTAB at a concentration of 10 mM at 100 and 60 °C, respectively, and the self-assembled ZnTPyP micro-rods (C). TEM images of the micro-prisms (D), micro-octahedra (E) and micro-rods (F).

with the help of CTAB (10 mM) as a surfactant. The high magnification SEM images of the micro-CPPs shown in Fig. S1A, 1B and 1C (ESI[†]) reveal the regular 3D micro-prism, micro-octahedron and micro-rod morphology of the micro-CPPs and additionally show that they have a smooth surface and a distinct outline formed at 100 and 60 °C for the micro-prisms and micro-octahedra, respectively. The transmission electron microscopy (TEM) images indicate the solid microstructures of the micro-prisms, micro-octahedra and micro-rods (Fig. 2D, 2E and 2F). Compared to the one-dimensional microstructure of the self-assembled ZnTPyP micro-rods, the obtained ZnTPyP micro-prisms and micro-octahedra show a typical three-dimensional architecture with sizes of about 477 ± 38 nm (width) \times 326 ± 51 nm (height) \times 0.97 ± 0.10 μ m (length) and 0.87 ± 0.08 μ m (side length) \times 544 ± 53 nm (height), respectively (inset of Fig. S2 in the ESI[†]).

Fig. 3A–D show the SEM images of the micro-prisms prepared at different concentration of CTAB while keeping the other experimental conditions constant. As shown in Fig. 3A, disordered and agglomerated particles were formed at 100 °C in the absence of CTAB in DMF. When a small amount of CTAB (3 mM) was introduced into the reaction system, deformed or cracked micro-scale ZnTPyP prisms, with an average size of *ca.* $1 \times 2 \times 5$ μ m, were obtained (Fig. 3B). Along with an increase in the CTAB concentration from 3 to 18 mM, a few individual ZnTPyP micro-prisms could be recognized from the three-dimensionally packed panel structures (Fig. 3C), which is presumably due to a growth/packing process prompted by the assistance of the surfactant and the intermolecular π - π stacking interaction. A further increase of the CTAB concentration to

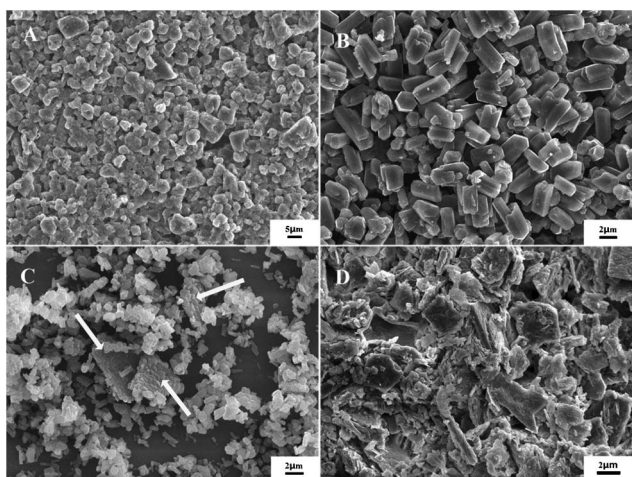


Fig. 3 SEM images of the micro-prisms formed at 100 °C with different CTAB concentrations of (A) 0 mM, (B) 3 mM, (C) 18 mM and (D) 30 mM.

30 mM resulted in irregular 3D blocks with a width of *ca.* 5~6 μm (Fig. 3D), which is due to ineffective aggregation and the assembly of an excessive amount of CTAB with the ZnTPyP micro-prisms.

The SEM images of the micro-octahedra prepared with different concentrations of CTAB are displayed in Fig. 4A–D. As expected, disordered and agglomerated particles were also formed at 60 °C in the absence of CTAB in DMF (Fig. 4A). As shown in Fig. 4B, when the concentration of CTAB was 3 mM, larger ZnTPyP micro-octahedra with a non-uniform size distribution were obtained compared to those obtained with the help of 10 mM surfactant CTAB (Fig. 2B).

When more CTAB (18 mM) was introduced into the reaction system, the ZnTPyP micro-octahedra began to transform into polyhedrons (Fig. 4C). A further increase in the CTAB concentration to 30 mM induced the formation of a large quantity of assembled 2D layered nano-plates (Fig. 4D). It appears that the surfactant can reduce the growth speed of the

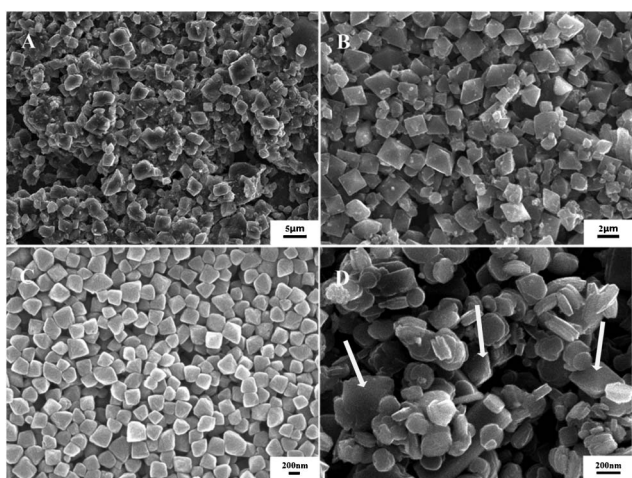


Fig. 4 SEM images of the micro-octahedra formed at 60 °C with different CTAB concentrations of (A) 0 mM, (B) 3 mM, (C) 18 mM and (D) 30 mM.

nanostructures and retard the fast aggregation and coordination process of the ZnTPyP molecules.^{19,20}

It can thus be noted that the presence of CTAB has a great influence on the morphology and size of the resulting CPP microstructures at a given temperature. With the addition of an appropriate amount of CTAB (10 mM), regular and ordered 3D ZnTPyP-CPP microstructures can be formed in DMF due to the cross-linking ability originating from the linear structure of CTAB. On the other hand, CTAB can be employed as a potential crystal face inhibitor in the reaction, which benefits the occurrence of oriented nucleation, resulting in the anisotropic growth of the micro-CPPs.²¹ However, the absence and the addition of an excessive amount of CTAB may result in the formation of irregular, agglomerated particles and disordered “blocky” agglomerates.

As a result, CTAB not only directs the growth/packing process of ZnTPyP into micro-prism and micro-octahedron structures but also controls the size distribution of the products. A delicate balance between the ZnTPyP–CTAB and ZnTPyP–ZnTPyP interactions seems to be satisfied when the concentration of CTAB is 10 mM and therefore results in uniform micro-prisms and micro-octahedra of ZnTPyP at the given temperature.

X-Ray Diffraction patterns

The internal structures of the ZnTPyP micro-coordination polymer particles (CPPs) and the self-assembled ZnTPyP micro-rods were investigated by X-ray diffraction (XRD). As can be seen in Fig. 5, both the CPPs with the different morphologies and the self-assembled ZnTPyP micro-rods exhibit similar XRD patterns. In particular, the micro-prisms and micro-octahedra show analogous XRD patterns with only slightly different intensities of (101), (011 overbar) and (201 overbar) peaks.

Nevertheless, the XRD patterns for all these three microstructures also correspond well to the simulated pattern on the basis of the crystal structure of ZnTPyP obtained by Goldberg *et al.* (CCDC ref. code YOVTOS), indicating the similar internal structure of the three microstructures to the single crystals, which have the space group $R\bar{3}$ and unit cell dimensions of $a = b = 33.110 \text{ \AA}$, $c = 9.374 \text{ \AA}$, $\alpha = \beta = 90^\circ$ and $\gamma = 120^\circ$.^{22–24} In these microstructures, the zinc atom at the center of ZnTPyP should be six-coordinated to four pyrrole nitrogens of the porphyrin core and to two pyridyl N-atoms of the other porphyrin molecules, which approach from both sides of the molecular framework. Obviously, the characteristic peak attributed to (220), which is designated from the ZnTPyP simulated pattern, is remarkably intense for self-assembled ZnTPyP micro-rods, while the (101) peak in the XRD pattern of the ZnTPyP micro-rods vanishes and the intensity of the peaks at (011 overbar) and (201 overbar) is significantly weakened compared with the simulated ones. These features indicate that ZnTPyP molecules in the self-assembled ZnTPyP micro-rods prefer to grow along the crystallographic c axis.^{11a} However, the (110) peak for both the micro-prisms and the micro-octahedra show a decreased intensity in comparison to both the simulated pattern and the self-assembled micro-rods, while the peaks assigned to (101), (011 overbar) and (201 overbar) are clearly more intense than the self-assembled micro-rods. It can be further observed that the relative intensity

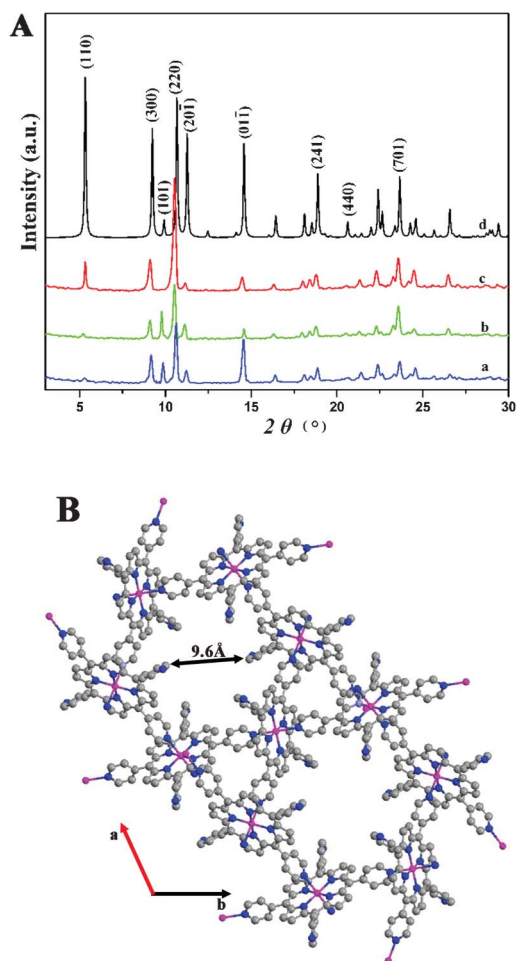


Fig. 5 (A) The XRD patterns of the micro-prisms (a), micro-octahedra (b) and the self-assembled ZnTPyP micro-rods (c) together with the simulated pattern (d) based on the published crystal structure data (CCDC ref. code: YOVTOS). (B) A space-filling representation of an open-framework structure of the CPPs along the crystallographic *c* axis: Zn, purple; N, blue; C, gray.

of the characteristic (011 overbar) peak in the micro-prisms (blue pattern) remarkable increases compared to that of the micro-octahedra (green pattern). These results reveal that ZnTPyP molecules grow and pack along the crystallographic *a*, *b* and *c* axes and the dominant growth is along the *b* axis in the micro-prisms and the *a* and *b* axes in the micro-octahedra.

Energy-dispersed X-ray (EDX) analysis

Energy-dispersed X-ray (EDX) spectroscopy was used to detect the composition of the samples as displayed in Fig. S3A–C (ESI†). The elemental signature for C, N and Zn in the EDX spectrum for the micro-prisms clearly indicates the composition of micro-prisms aside from ZnTPyP. The additional elemental signatures of the O and Si atoms come from the substrate (Fig. S3A of the ESI†). The atomic ratio, N : Zn, for the micro-prisms is nearly 8 : 1, which is in agreement with the composition of ZnTPyP. This is also true for the micro-octahedra and self-assembled ZnTPyP micro-rods (Fig. S3B and S3C of the ESI†).

FT-IR spectra

The FT-IR spectra of ZnTPyP, the micro-prism CPPs, the micro-octahedra CPPs and the self-assembled micro-rods are compared in Fig. 6

The similar features of the IR spectra of the micro-sized CPPs, the self-assembled ZnTPyP micro-rods and ZnTPyP unambiguously confirm the composition of the micro-prisms, micro-octahedra and self-assembled ZnTPyP micro-rods from ZnTPyP. The characteristic strong band at 1604 cm^{-1} , due to the C=N stretching vibration of the *meso*-attached pyridyl substituents in ZnTPyP, splits into two peaks observed at 1620 and 1594 cm^{-1} for the micro-prisms and at 1623 and 1598 cm^{-1} for the micro-octahedra, indicating the formation of a Zn–N metal–ligand coordination between the *meso*-attached pyridyl substituents in the porphyrin molecule with the zinc center of a neighboring molecule in the microstructure of the CPPs.²⁵ This is also true for the self-assembled ZnTPyP micro-rods, as revealed by the splitting of the C=N stretching vibration bands at 1632 and 1600 cm^{-1} . However, these micro-CPPs showed a shift of their IR peak positions to lower wavenumbers in comparison to the self-assembled ZnTPyP micro-rods, indicating the relatively higher degree of ordering and firm Zn–N coordination aggregates in these micro-CPPs.²⁶

Luminescent properties

The photoluminescence (PL) emission spectrum of ZnTPyP in DMF together with those of its self-assembled micro-rods, micro-prisms and micro-octahedra are shown in Fig. 7. As can be seen, upon excitation at the ZnTPyP Soret band wavelength (around 425 nm), ZnTPyP in DMF shows two intense emission bands at 609 and 653 nm together with a weak band at *ca.* 722 nm (Fig. 7a). Upon reaction to form the self-assembled micro-rods, red-shifted emission bands with similar features to those of ZnTPyP in solution were observed in the photoluminescence emission spectrum shown in Fig. 7b. A red-shift of the main emission band was also seen for the micro-prisms and micro-octahedra

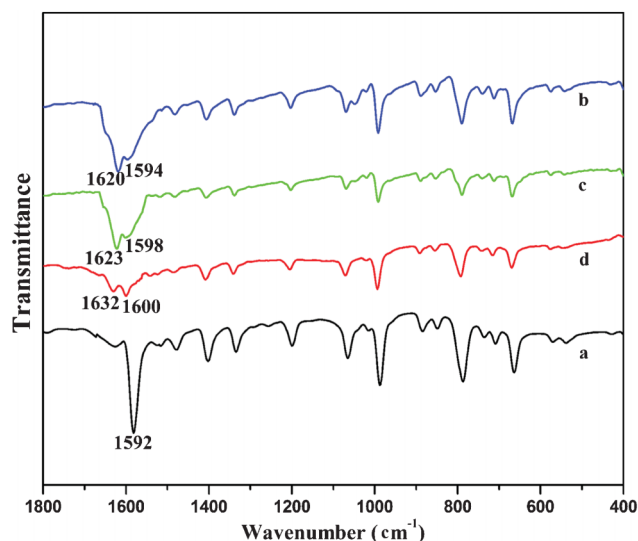


Fig. 6 The FT-IR spectra of ZnTPyP (a), micro-prisms (b), micro-octahedra (c) and the ZnTPyP micro-rods (d).

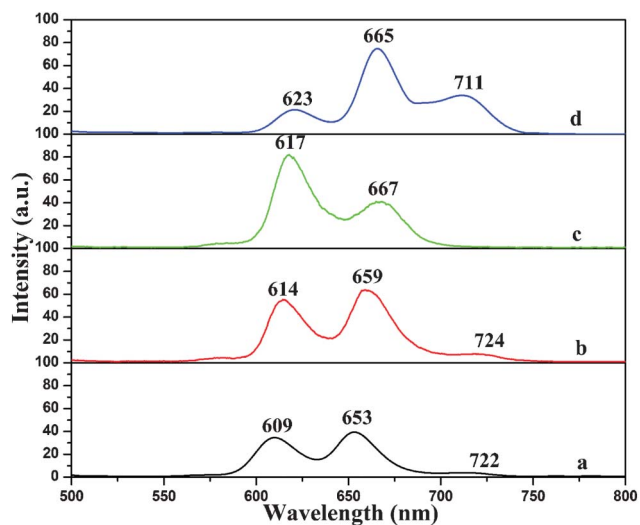


Fig. 7 The fluorescence spectrum of ZnTPyP in DMF (a) together with those of self-assembled ZnTPyP micro-rods (b), micro-prisms (c) and micro-octahedra (d) dispersed in water upon excitation at 425 nm.

(Fig. 7c and 7d), which corresponds to J-type aggregates and is in good agreement with the UV-vis experimental results described above. However, the weaker band disappears in the micro-prism spectrum, while the weak band in the micro-octahedra spectrum becomes more intense. Due to the same coordination patterns observed in the ZnTPyP micro-particles, the morphology-dependent optical properties in the present case imply an effect of both the concentration of the surfactant, CTAB, and the reaction temperature on the intermolecular stacking.²⁷

Adsorption properties

Fig. 8 shows the nitrogen adsorption/desorption isotherms and corresponding micropore size distributions of the different ZnTPyP microstructures. The nitrogen isotherms shown in Fig. 8A are characteristic of the type I isotherm without an apparent hysteresis and they can be used to indicate the micropore size of the self-assembled micro-rods, micro-prisms and micro-octahedra of ZnTPyP Fig. 8B.²⁸

This result was confirmed by the calculated pore size, which was in the range of 7.1–8.8 Å for the three microstructures fabricated from ZnTPyP (Table 2). BET measurements led to the relatively larger surface area for the micro-prisms and micro-octahedra (138.31 and 79.11 m² g⁻¹) relative to 38.23 m² g⁻¹, which was found for the self-assembled micro-rods of ZnTPyP. This indicates the improved potential of the former two CPP microstructures in the field of gas adsorption.

This result was further supported by the larger porosity of both the micro-prisms and the micro-octahedra compared to that of the self-assembled ZnTPyP micro-rods (Table 2). In addition, the pore size distribution shows a major peak around ~0.8 nm (Fig. 8B). This corresponds well to the hexagonal crystal lattice simulation based on the published crystal structure data as mentioned above. Nevertheless, the porosity of these three microstructures is still well maintained after degassing at 70 °C for 48 h, suggesting the relatively higher stability of the pore structures.

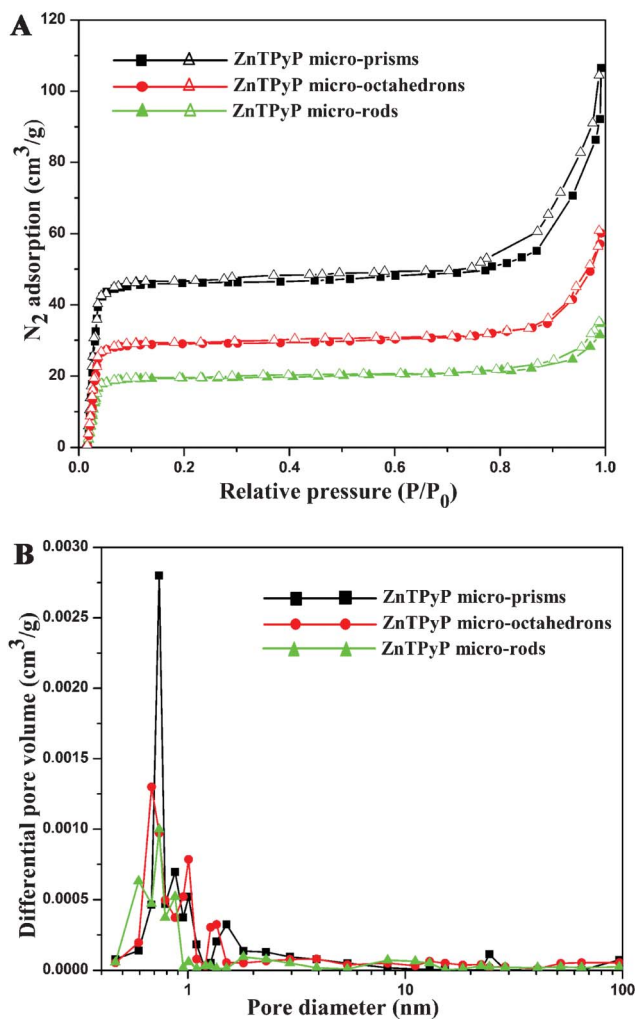


Fig. 8 (A) The nitrogen sorption isotherms obtained at 77 K for ZnTPyP micro-prisms, ZnTPyP micro-octahedra and the self-assembled ZnTPyP micro-rods after degassing at 343 K for 48 h. (B) The micropore size distributions for the ZnTPyP micro-prisms, ZnTPyP micro-octahedra and self-assembled ZnTPyP micro-rods.

Table 2 The porosity, surface area and pore size of the different ZnTPyP microstructures

Compound	Porosity (%)	Surface area (m ² g ⁻¹)	Pore size (Å)
micro-prisms	27.3	138.31	8.8
micro-octahedra	15.8	79.11	7.3
micro-rods	7.4	38.23	7.1

Conclusion

Three-dimensional microstructured ZnTPyP coordination polymer particles (CPPs) with prism-like and octahedral morphologies and uniform sizes have been controllably prepared by a surfactant-assisted reaction. The concentration of surfactant (CTAB) and the reaction temperature were revealed to play a vital role in the formation and growth process of the micro-CPPs, which led to the formation of three dimensional micro-prisms and micro-octahedra prompted by the crystal packing force and π - π stacking interactions at a given temperature. In

addition, the two ZnTPyP CPPs show better luminescent properties and N₂ absorption properties due to the larger surface area and porosity of the micro-CPPs. They may be valuable in the design and preparation of size- and morphology-adjustable micro-CPP materials for micro-scale molecular (opto)-electronic devices that often require a wide variety of channel sizes to achieve the optimum optical modulation.

Acknowledgements

Financial support from the Natural Science Foundation of China, the Ministry of Education of China, the Beijing Municipal Commission of Education, the Fundamental Research Funds for the Central Universities and the University of Science and Technology, Beijing is gratefully acknowledged.

References

- 1 W. Cho, H. J. Lee and M. Oh, *J. Am. Chem. Soc.*, 2008, **130**, 16943.
- 2 L. H. Wee, S. R. Bajpe, N. Janssens, I. Hermans, K. Houthoofd, C. E. A. Kirschhock and J. A. Martens, *Chem. Commun.*, 2010, **46**, 8186.
- 3 M. Oh and C. A. Mirkin, *Angew. Chem., Int. Ed.*, 2006, **45**, 5492.
- 4 M. Oh and C. A. Mirkin, *Nature*, 2005, **438**, 651.
- 5 P. Horcajada, C. Serre, M. Vallet-Regí, M. Sebban, F. Taulelle and G. Férey, *Angew. Chem., Int. Ed.*, 2006, **45**, 5974.
- 6 A. Facchetti, *Mater. Today*, 2007, **10**, 28.
- 7 A. L. Briseno, S. C. B. Mannsfeld, S. A. Jenekhe, Z. Bao and Y. Xia, *Mater. Today*, 2008, **11**, 38.
- 8 A. C. Grimsdale and K. Müllen, *Angew. Chem., Int. Ed.*, 2005, **44**, 5592.
- 9 D. Horn and J. Rieger, *Angew. Chem., Int. Ed.*, 2001, **40**, 4330.
- 10 (a) K. M. L. Taylor, W. J. Rieter and W. Lin, *J. Am. Chem. Soc.*, 2008, **130**, 14358; (b) W. J. Rieter, K. M. Pott, K. M. L. Taylor and W. Lin, *J. Am. Chem. Soc.*, 2008, **130**, 11584; (c) K. M. L. Taylor, A. Jin and W. Lin, *Angew. Chem., Int. Ed.*, 2008, **47**, 7722.
- 11 (a) X. Sun, S. Dong and E. Wang, *J. Am. Chem. Soc.*, 2005, **127**, 13102; (b) S. Jung and M. Oh, *Angew. Chem., Int. Ed.*, 2008, **47**, 2049; (c) H. J. Lee, W. Cho, S. Jung and M. Oh, *Adv. Mater.*, 2009, **21**, 674; (d) S. Jung, W. Cho, H. J. Lee and M. Oh, *Angew. Chem., Int. Ed.*, 2009, **48**, 1459.
- 12 (a) Z. Ni and R. I. Masel, *J. Am. Chem. Soc.*, 2006, **128**, 12394; (b) N. S. John, C. Scherb, M. Shōāēē, M. W. Anderson, M. P. Attfield and T. Bein, *Chem. Commun.*, 2009, 6294.
- 13 H. J. Lee, W. Cho and M. Oh, *CrystEngComm*, 2010, **12**, 3959.
- 14 (a) I. Goldberg, *Chem.–Eur. J.*, 2000, **6**, 3863; (b) I. Goldberg, *Chem. Commun.*, 2005, 1243; (c) I. Goldberg, *CrystEngComm*, 2008, **10**, 637; (d) L. D. DeVries and W. J. Choe, *J. Chem. Crystallogr.*, 2009, **39**, 229; (e) P. M. Barron, H. Son, C. Hu and W. Choe, *Cryst. Growth Des.*, 2009, **9**, 1960; (f) H. Chung, P. M. Barron, R. W. Novotny, H. Son, C. Hu and W. Choe, *Cryst. Growth Des.*, 2009, **9**, 3327; (g) I. Beletskaya, V. S. Tyurin, A. Y. Tsivadze, R. Guillard and C. Stern, *Chem. Rev.*, 2009, **109**, 1659; (h) R. W. Seidel and I. M. Oppel, *Struct. Chem.*, 2009, **20**, 121.
- 15 (a) J. S. Hu, Y. G. Guo, H. P. Liang, L. J. Wan and L. Jiang, *J. Am. Chem. Soc.*, 2005, **127**, 17090; (b) Y. F. Qiu, P. L. Chen and M. H. Liu, *J. Am. Chem. Soc.*, 2010, **132**, 9644; (c) L. Pan, X. Y. Huang, H. N. Phan, T. J. Emge, J. Li and X. T. Wang, *Inorg. Chem.*, 2004, **43**, 6878; (d) J. L. Ruggles, G. J. Foran, H. Tanida, H. Nagatani, Y. Jimura, I. Watanabe and I. R. Gentle, *Langmuir*, 2006, **22**, 681.
- 16 F. Bai, H. M. Wu, R. E. Haddad, Z. C. Sun, S. K. Schmitt, V. R. Skocypc and H. Y. Fan, *Chem. Commun.*, 2011, **47**, 5055.
- 17 N. C. Maiti, S. Mazumdar and N. J. Periasamy, *J. Phys. Chem. B*, 1998, **102**, 1528.
- 18 S. Okada and H. Segawa, *J. Am. Chem. Soc.*, 2003, **125**, 2792.
- 19 (a) Q. Zhou, C. M. Li, J. Li and J. Lu, *J. Phys. Chem. C*, 2008, **112**, 18578; (b) Q. Zhou, C. M. Li, J. Li, X. Cui and D. Gervasio, *J. Phys. Chem. C*, 2007, **111**, 11216.
- 20 M. F. Casula, Y. W. Jun, D. J. Zaziski, E. M. Chan, A. Corrias and A. P. Alivisatos, *J. Am. Chem. Soc.*, 2006, **128**, 1675.
- 21 Y. G. Zhang, S. T. Wang, X. B. Li, L. Y. Chen, Y. T. Qian and Z. D. Zhang, *J. Cryst. Growth*, 2006, **291**, 196.
- 22 S. H. Im, U. Jeong and Y. Xia, *Nat. Mater.*, 2005, **4**, 671.
- 23 H. Krupitsky, Z. Stein, I. Goldberg and C. E. J. Strouse, *J. Inclusion Phenom. Mol. Recognit. Chem.*, 1994, **18**, 177.
- 24 K. J. Lin, *Angew. Chem., Int. Ed.*, 1999, **38**, 2730.
- 25 G. Lu, X. Zhang, X. Cai and J. Jiang, *J. Mater. Chem.*, 2009, **19**, 2417.
- 26 T. Nakanishi, B. Ohtani and K. Uosaki, *J. Phys. Chem. B*, 1998, **102**, 1571.
- 27 E. Kwon, H. R. Chung, Y. Araki, H. Oikawa, O. Ito and H. Nakanishi, *Chem. Phys. Lett.*, 2007, **441**, 106.
- 28 (a) K. M. Ok, J. Sung, G. Hu, R. M. J. Jacobs and D. O'Hare, *J. Am. Chem. Soc.*, 2008, **130**, 3762; (b) D. N. Dybtsev, H. Chun, S. H. Yoon, D. Kim and K. Kim, *J. Am. Chem. Soc.*, 2004, **126**, 32.